Methane Combustion over Pd/Al_2O_3 Catalysts in the Presence of Water: Effects of Pd Particle Size and Alumina Crystalline Phase

Kazumasa Murata[†], *Junya Ohyama*[‡, §], *Yuta Yamamoto*[∥], *Shigeo Arai*[∥], *Atsushi Satsuma*[†, §, *]

[†]Graduate School of Engineering, Nagoya University, Nagoya 464-8603, Japan

[‡]Faculty of Advanced Science and Technology, Kumamoto University, Kumamoto 860-8555, Japan

[∥]Institute of Materials and Systems for Sustainability, Nagoya University, Nagoya 464-8603, Japan

[§]Elements Strategy Initiative for Catalysts and Batteries (ESICB), Kyoto University, Katsura, Kyoto 615-8520, Japan

ABSTRACT

The effects of the Pd particle size and the Al_2O_3 crystalline phase of Pd/Al_2O_3 catalysts on the CH_4 combustion in the presence of H_2O were investigated. According to X-ray absorption fine structure (XAFS)

measurements, it was revealed that, during the CH_4 combustion, the Pd nanoparticles existed on the Al_2O_3 support as a PdO phase, while the crystallinity of PdO depended on the Pd particle size. Based on X-ray diffraction (XRD), amorphous PdO particles with a size of <7 nm exhibited low activity for CH_4 combustion. In contrast, as the Pd particle size increased, larger crystalline PdO particles (>7 nm) were formed, which were highly active for CH_4 combustion. Comparing the effects of the different Al_2O_3 crystalline phases, Pd/α-Al_2O_3 was proved to be more resistant to deactivation by H_2O than Pd/γ-Al_2O_3 and Pd/θ-Al_2O_3. Moreover, according to H_2O temperature-programmed desorption (TPD) and infrared (IR) measurements, since α-Al_2O_3 was relatively hydrophobic compared to γ-Al_2O_3 and θ-Al_2O_3, a faster and reversible adsorption/desorption of OH/H_2O species was achieved, while the H_2O-poisoning on PdO species in the vicinity was limited.

KEYWORDS: methane combustion, Pd catalyst, alumina, particle size, crystalline phase

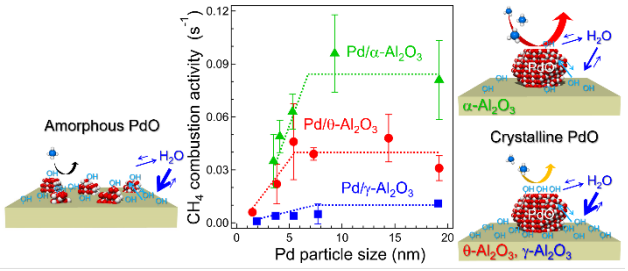

1. INTRODUCTION

Natural gas, which consists mainly of methane (CH_4), is increasingly being used as a fuel for natural gas vehicles and thermal power production. When used as a fuel, its exhaust gas contains a considerable amount of

unburned CH_4, which has a greenhouse effect 25 times higher than that of CO_2. Supported Pd catalysts have been widely used for complete combustion of CH_4 that would require conversion of unburned CH_4 into CO_2 and H_2O.[1] During CH_4 combustion under oxygen excess, Pd is easily oxidized to an active PdO phase.[2–4] Previous studies on the effect of supports on the efficiency of supported Pd catalysts suggested that Al_2O_3 is one of the most effective supports for CH_4 combustion due to the charge transfer between Pd and Al_2O_3 that improves the redox properties of the Pd particles.[5–10] Our research group has investigated the effect of different Al_2O_3 crystalline phases on CH_4 combustion under water-free (dry) conditions over Pd/Al_2O_3 prepared by the impregnation method.[10] It was revealed that the Al_2O_3 crystal phase with different interaction strengths with Pd triggered the structural change of the Pd particles, which are precursors of the active PdO phase. On γ-Al_2O_3, which strongly interacts with Pd, the Pd particles displayed an amorphous-like surface with abundant corner sites and exhibited low activities for CH_4 combustion. Instead, their weak interaction with θ- and α-Al_2O_3 resulted in the formation of spherical Pd particles with a high fraction of highly active step sites.

Nevertheless, it should be considered that the exhaust gas in a catalytic converter contains in addition to low CH_4 concentrations (400–1500 ppm), high concentrations of H_2O vapors (10–15%),[11] which strongly interferes with the CH_4 combustion over Pd catalysts. Therefore, the development of a catalyst with high CH_4 combustion activity even in the presence of H_2O (wet conditions) is an imperative need. So far, several mechanisms have been reported for the deactivation mechanism of CH_4 combustion by H_2O. In particular, it has been suggested that the adsorption of OH/H_2O species on active PdO reduces the number of active sites

that could participate in the CH_4 activation,[5,12–16] while the accumulation of OH/H_2O species on the catalyst supports may impair the oxygen supply between Pd and the support.[17–20] In addition, at high temperatures (>500 °C), sintering of PdO particles was induced in the presence of H_2O vapors.[11,21,22] Therefore, the selection of the appropriate catalyst support is important for the development of highly active Pd catalysts for CH_4 combustion under wet conditions. So far, Pd catalysts with good hydrothermal durability have been developed using ZrO_2.[23,24] The addition of CeO_2, which has high oxygen mobility, suppressed the negative effect of H_2O on the activity[20], while the SnO_2 support promoted the release of OH species from the active PdO surface and exhibited high activity even in the presence of H_2O.[12] In the case of a Pd/zeolite catalyst, the high Si/Al ratio improved the H_2O resistance during CH_4 combustion due to its superior hydrophobicity.[13,25] Pd/Al_2O_3 catalysts have exhibited high activity for CH_4 combustion under dry conditions, but their relative hydrophilicity leads to considerable deactivation by H_2O.[12,26] Therefore, since Al_2O_3 is present in various crystal phases, such as γ, θ, and α, their effect on CH_4 combustion in the presence of H_2O should be further investigated. Differences in the surface Al^{3+} sites and OH groups of Al_2O_3, derived from the crystalline phase, are expected to affect the interaction between the Pd/Al_2O_3 catalyst and H_2O.[27,28]

The Pd particle size effect on CH_4 combustion under dry conditions has been studied. Under dry conditions, an under-coordinated PdO surface such as PdO(101) is known to be more active for CH_4 combustion than a well-coordinated PdO(100) surface.[29] It has been proposed that the proportion of Pd(101) on PdO particles was depended on the Pd particle size.[5,10] However, the PdO(101) surface is possible to be strongly deactivated by

water.[30] Therefore, the effect of Pd particle size on CH_4 combustion in the presence of H_2O should be studied.

Herein, we systematically investigated the CH_4 combustion activities under wet conditions of Pd/Al_2O_3 catalysts with different Pd particle size and Al_2O_3 crystal phase. The crystallinity of active PdO phase depended on the Pd particle size. Comparison of the catalytic activities in the presence and absence of H_2O indicated a different effect of the Al_2O_3 support on the deactivation by H_2O. Moreover, based on kinetic analysis and spectroscopic data, the deactivation factors during CH_4 combustion could be explored at low temperature (350 °C). The role of the Al_2O_3 support indirectly involved in CH_4 combustion over a Pd catalyst was also mentioned.

2. RESULTS AND DISCUSSION

2.1 Catalyst preparation and Pd particle size

Al_2O_3 with different crystal phases (γ-Al_2O_3, θ-Al_2O_3, and α-Al_2O_3) was used as a support for the Pd catalysts. The Al_2O_3 supported Pd catalyst were prepared by the impregnation method. The ^{27}Al magic angle spin nuclear magnetic resonance spectra of Al_2O_3 with different crystal phases have been reported in our previous study,[10] and the crystalline phases of Al_2O_3 were identified by X-ray diffraction (XRD) (Figure 1). The Brunauer–Emmett–Teller (BET) specific surface areas of Al_2O_3 are provided in Table 1. The PdO particle size of Pd/Al_2O_3 was changed by tuning the Pd loading (0.2–2wt%) or the calcination temperature (800–900 °C). The average PdO particle size was estimated by CO adsorption, H_2 adsorption, and scanning transmission electron microscopy (STEM) measurements of the metallic Pd particles after the reduction

pretreatment of the catalysts, as the Pd particle size was not significantly affected by the chemical state.[31] The Pd particle sizes of Pd/Al_2O_3 catalysts are outlined in Table S1.[10,32] The catalysts were denoted as X nm Pd/Al_2O_3, where X represents the average Pd particle size of Pd/Al_2O_3 estimated by CO adsorption.

Table 1. The BET surface area and the water desorption amount of alumina supports.

Samples	BET surface area ($m^2\ g^{-1}$)	Desorption amount of water ($mmol\ g^{-1}$)			Desorption amount of water per surface area ($10^{-3}\ mmol\ m^{-2}$)		
		First peak (at 50–500 °C)	Second peak (at 500–800 °C)	Total	First peak (at 50–500 °C)	Second peak (at 500–800 °C)	Total
γ-Al_2O_3	204	1.178	0.198	1.376	5.78	0.97	6.75
θ-Al_2O_3	73	0.176	0.031	0.207	2.41	0.43	2.84
α-Al_2O_3	10	0.051	0.003	0.054	5.10	0.30	5.40

2.2 XRD analysis

As observed in the XRD patterns of the Pd/Al_2O_3 catalysts (Figure 1), for 1.9 nm Pd/γ-Al_2O_3 (Figure 1a) and 1.5 nm Pd/θ-Al_2O_3 (Figure 1b), only the diffraction peaks of the Al_2O_3 supports could be detected. However, as the Pd particle size increased, the diffraction peaks derived from PdO appeared and their intensities increased, implying that crystalline PdO particles were formed on the Al_2O_3 support as the Pd particle size increased. In contrast, the diffraction peak of Pd metal was not observed in any of the currently examined Pd/Al_2O_3 catalysts. Based on the line intensity at 33.9° illustrated in Figure 2, the diffraction intensities of PdO increased in two steps with the increase in the Pd particle size of all the Pd/Al_2O_3 catalysts. In particular, a sharp increase in PdO diffraction intensity at <7 nm indicated the formation of crystalline PdO particles from highly dispersed PdO species, while at sizes >7 nm, a gradual increase in the PdO intensity suggested the growth of the already formed crystalline PdO particles.

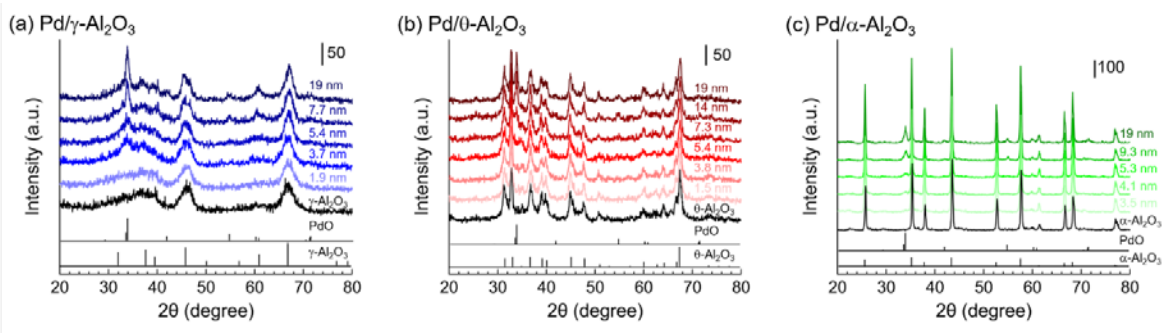

Figure 1. XRD patterns of (a) Pd/γ-Al_2O_3, (b) Pd/θ-Al_2O_3, and (c) Pd/α-Al_2O_3 with PDF cards of Al_2O_3 and PdO (PDF number #02-1420, #35-0121, #10-0173, and #43-1024).

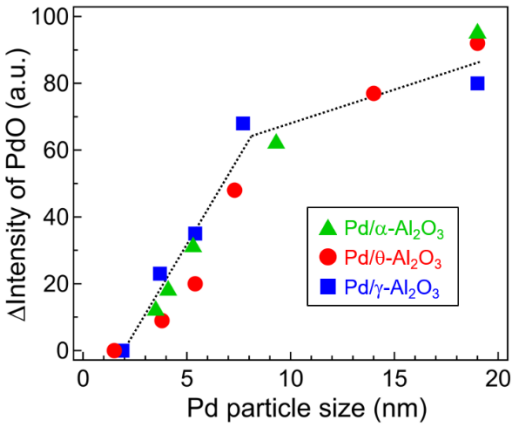

Figure 2. Dependence of the Δintensity of PdO on the Pd particle size, derived from the XRD patterns. The Δintensity of PdO was calculated by subtracting the intensity of Al_2O_3 from the intensity of Pd/Al_2O_3 at 33.9°.

2.3 Pd-K-edge XAFS spectroscopy

The oxidation state and local structure of the Pd species on Al_2O_3 were investigated by X-ray absorption fine structure (XAFS) measurements. The Pd K-edge X-ray absorption near edge structure (XANES) spectra of all Pd/Al_2O_3 catalysts were consistent with that of the PdO reference (Figure 3 top), indicating that the Pd particles on Al_2O_3 supports were completely oxidized to PdO. Furthermore, based on the Fourier transforms of extended X-ray absorption structure (FTs of EXAFS) spectra of Pd/Al_2O_3 (Figure 3 bottom), the Pd–O and

Pd–Pd scattering peaks were observed at around 1.6 and 3.0 Å, respectively. As the Pd particle size decreased, the Pd–Pd scattering peak intensity around 3.0 Å decreased. In addition, no Pd–Pd scattering peak derived from PdO was observed near 3.0 Å for 1.9 nm Pd/γ-Al_2O_3 and 1.5 nm Pd/θ-Al_2O_3, suggesting that isolated Pd atoms and amorphous-like PdO particles were mainly present in the Pd/Al_2O_3 catalysts with smaller Pd particle size. The coordination number of Pd–Pd in PdO obtained by EXAFS fitting was also plotted on the particle size (Figure S1 and Table S2), revealing that it increased with increasing Pd particle size. Moreover, it is clear that the increase in the coordination number of Pd–Pd in PdO was remarkable below 7 nm, corresponding to the formation of crystalline PdO particles.

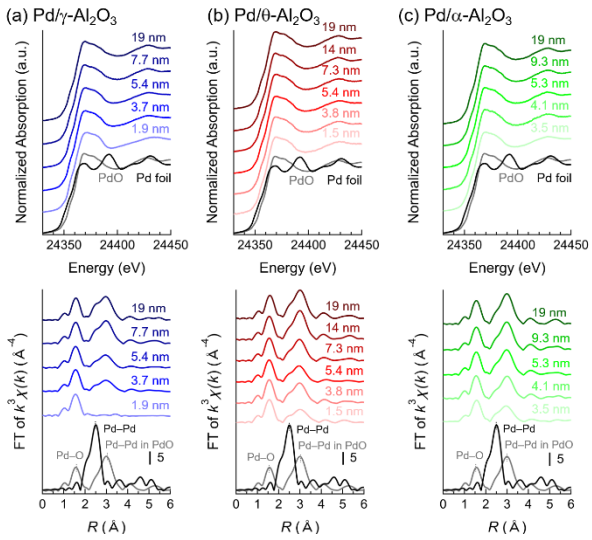

Figure 3. Pd K-edge XANES (top) and FTs of EXAFS (bottom) spectra before CH_4 combustion for Pd/Al_2O_3 with different Pd particle sizes. The black and gray lines indicate the Pd foil and PdO references, respectively.

2.4 STEM analysis

According to the STEM images of PdO particles on θ-Al_2O_3, when the Pd particle size was less than 3 nm,

the contrast of PdO particles relative to those of Al_2O_3 was unclear and no lattice fringes of PdO were observed (Figure 4a). Therefore, at small Pd particle sizes (<3 nm), the PdO particles formed an amorphous-like structure. In comparison, PdO particles with size greater than 10 nm clearly displayed lattice fringes derived from PdO (101), indicating the high crystallinity of PdO (Figure 4b).

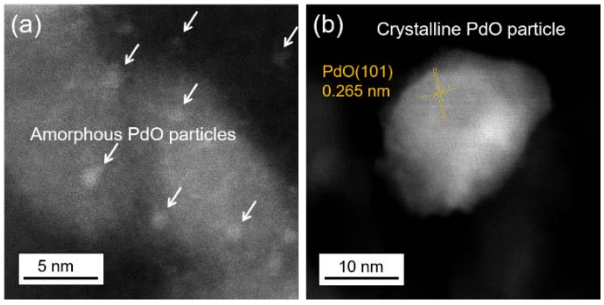

Figure 4. STEM images of (a) <3 nm and (b) >10 nm Pd particles supported on θ-Al_2O_3 after CH_4 combustion. The white arrows indicate the positions of the <3 nm Pd particles.

2.5 Evaluation of the CH_4 combustion activity

The activity of the CH_4 conversion under wet conditions (0.4% CH_4, 10% O_2, 12% H_2O and N_2 balance) was tested over Pd/Al_2O_3 with different Al_2O_3 crystal phases at a temperature range from 300 to 600 °C (Figure S2). The CH_4 conversions over 5.4 nm Pd/θ-Al_2O_3 and 9.3 nm Pd/α-Al_2O_3 under wet conditions ignited at around 300 °C and reached approximately 100% at 450 ℃. Despite the larger Pd particle size, the CH_4 combustion activity of 9.3 nm Pd/α-Al_2O_3 was almost identical to that of 5.4 nm Pd/θ-Al_2O_3. In contrast, the CH_4 conversion over the 3.7 nm Pd/γ-Al_2O_3 catalyst was about 90% at 600 °C. Thus, the CH_4 combustion activity of Pd/Al_2O_3 catalysts under wet conditions shifted to a higher temperature by 50–100 °C compared to

that under dry conditions, due to the presence of H_2O.[10]

The effect of the Pd particle size and the Al_2O_3 crystalline phase on the CH_4 combustion activity in the presence of H_2O was also investigated. The turnover frequency of the catalysts under wet conditions (TOF_{wet}) was calculated for a CH_4 conversion of <20% to exclude the heat and gas diffusion problems in kinetic analysis.[10] According to the results of the dependence of TOF_{wet} on the Pd particle size at 350 °C under wet conditions (Figure 5a), all Pd/Al_2O_3 catalysts showed a similar trend regardless of the Al_2O_3 crystalline phase. In the particle size region from 1 to 7 nm, TOF_{wet} increased monotonically with increasing particle size. However, for particle sizes greater than 7 nm, the TOF_{wet} remained almost constant. According to the structure of the PdO particles obtained from XRD, XAFS, and STEM results, the Pd single atoms and amorphous-like PdO particles decreased with increasing particle size in the region up to 7 nm, and crystalline PdO particles were formed. Figure 5b shows the dependence of the CH_4 combustion activity (wet conditions, 350 °C) per total Pd molar in the Pd catalyst on the Pd particle size. The maximum activities were obtained at about 5 nm because the fraction of Pd surface atom decreased with increasing Pd particle size. The comparison of the activity of Pd catalysts reported in previous studies and the current work was not simple because of the different Pd loading, H_2O concentration, and gas hourly space velocity (GHSV). However, the catalytic activity of 9.3 nm Pd/α-Al_2O_3 was comparable or higher than that of other reported Pd catalysts, despite this study achieved high H_2O concentration and GHSV values (Table S3).[7,13,21,23–26,33,34]

TOF_{wet} was also plotted against the XRD intensity of PdO to clarify the relationship between the structure

of PdO and the CH_4 combustion activity (Figure S3). More specifically, it was observed that when the XRD intensity of PdO increased from zero to about 40, TOF_{wet} increased monotonically. Moreover, TOF_{wet} increased with the increase in the Pd–Pd coordination number in PdO, estimated from the curve fitting of the EXAFS spectra (Figure S4). Therefore, crystalline PdO particles were more active in CH_4 combustion in the presence of H_2O than isolated Pd atoms and amorphous-like PdO particles. This size effect could be attributed to the promotion of the C–H activation of methane on PdO ensembles such as PdO(101).[29,35] In the size region of >7 nm, the TOF under dry conditions slightly decreased as the particle size increased, but the TOF_{wet} under wet conditions was constant.[9,10] This difference indicated that the active PdO(101) surface was more strongly deactivated than the PdO(100) surface by water. Thus, the CH_4 combustion activity of PdO(101) surface may be similar to that of PdO(100) under wet conditions. As for the dependence on the Al_2O_3 crystal phases, the TOF_{wet} of Pd/α-Al_2O_3 was nine times that of Pd/γ-Al_2O_3 and twice that of Pd/θ-Al_2O_3 at sizes greater than 7 nm.

Furthermore, the change in $\ln(TOF_{wet}/TOF_{dry})$ over the Pd particle size was explored (Figure 5c). The TOF_{dry} value was estimated in our previous study from the CH_4 combustion rate at 300 °C under dry conditions,[10] where only a small amount of H_2O was generated form CH_4. The smaller $\ln(TOF_{wet}/TOF_{dry})$ value in Figure 5c indicated a greater decrease of the activity due to the presence of H_2O. In particular, the $\ln(TOF_{wet}/TOF_{dry})$ value of Pd/α-Al_2O_3 was about −1, regardless of the particle size, and was greater than the values of Pd/γ-Al_2O_3 and Pd/θ-Al_2O_3, which ranged from around −2 to −3 and were also not significantly

affected by the Pd particle size. The time courses of the CH_4 combustion over Al_2O_3-supported Pd particles, prepared by the colloidal method with similar size and shape,[9] were also compared (Figure S5). The decay in normalized TOF_{wet} of Pd/α-Al_2O_3 was smaller than that of Pd/γ-Al_2O_3 and Pd/θ-Al_2O_3, indicating that the CH_4 combustion activity of Pd/α-Al_2O_3 was less inhibited by H_2O vapors. Moreover, given that the $\ln(TOF_{wet}/TOF_{dry})$ value is independent of the Pd particle size (Figure 5c), the Al_2O_3 support would regulate the tolerance to H_2O vapors. It has been reported that the accumulation of H_2O and OH groups on the support hinders the supply of oxygen species from the support to the PdO lattice or the Pd surface,[17–19] thus decreasing the CH_4 combustion activity. Therefore, it is expected that the CH_4 combustion activities will decrease as the Pd particle size increases, that is, the Pd–Al_2O_3 interface sites decrease. But, the constant $\ln(TOF_{wet}/TOF_{dry})$ value over the change in the Pd particle size suggested that the H_2O-inhibited oxygen supply between Pd and the Al_2O_3 support was not the main factor for the decrease in the catalytic activity.

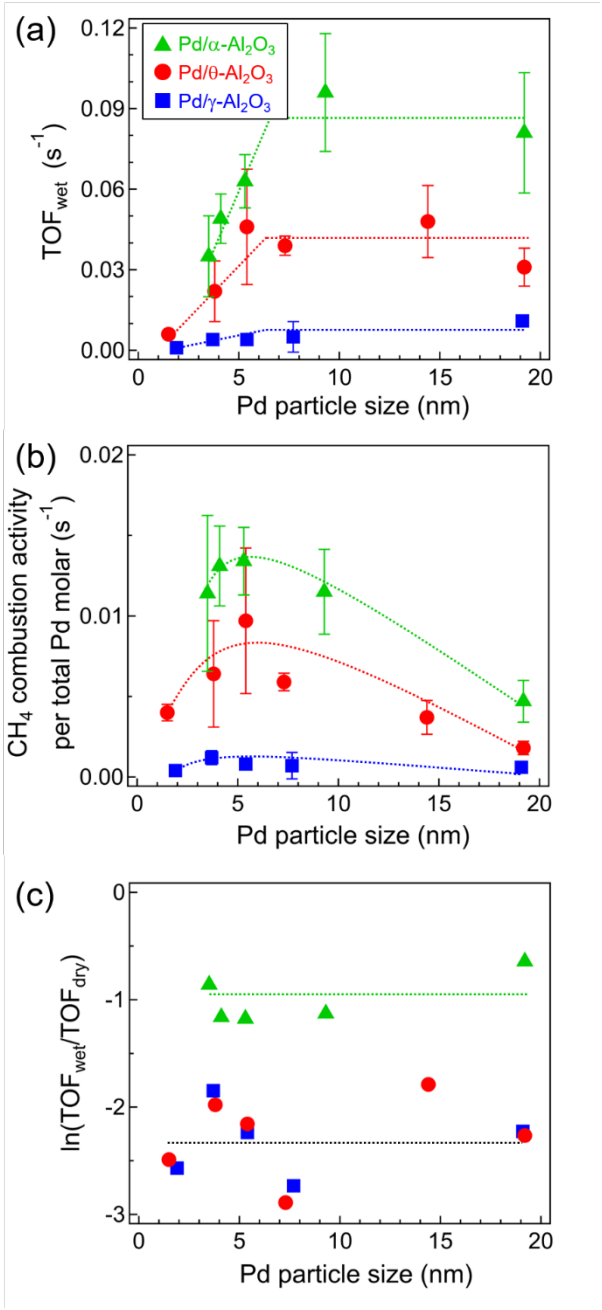

Figure 5. Dependence of (a) TOF_{wet} at 350 °C (b) CH_4 combustion activity per total Pd molar at 350 °C, and (c) $\ln(TOF_{wet}/TOF_{dry})$ on Pd particle size. Reaction conditions: 0.4% CH_4, 10% O_2, 12% H_2O and N_2 balance, 100 mL min^{-1}, GHSV 300,000 mL g^{-1} h^{-1}.

The structural change of the Pd/Al_2O_3 catalysts after CH_4 combustion in the presence of H_2O was

confirmed using XAFS measurements (Figure S6). Based on the Pd-K-edge XANES spectrum, Pd was present on the Al_2O_3 support as an active PdO species after CH_4 combustion. While the FTs of EXAFS spectra of Pd/Al_2O_3 were not significantly changed by the CH_4 combustion. The results indicated that the decrease in the catalytic activities under wet conditions was not by the change in the oxidation state and the local structure of PdO particles. According to *in situ* XAFS measurements, the PdO phase was maintained during CH_4 combustion at <600 °C.[4,36] Above 600 °C, PdO was thermally decomposed to Pd metal. On the other hand, when the CH_4 combustion was initiated using the Pd catalyst in the metal state, the Pd metal was oxidized to PdO with increasing temperature.[2,37,38] In addition to, thermodynamics of Pd−PdO phase transitions showed that the PdO phase was stable during CH_4 combustion.[3] These reports were consistent with the maintenance of the PdO phase before and after CH_4 combustion in this study.

2.6 Kinetic analysis of methane combustion under wet conditions

The apparent activation energy of CH_4 combustion in the presence of H_2O was estimated using the Arrhenius plot (Figure S7). According to the plot of the apparent activation energy over the particle size (Figure S8), the apparent activation energy was 111–177 kJ mol^{-1}, while no dependence on the Pd particle size or the Al_2O_3 support was identified. The results were consistent with an earlier report,[5] suggesting that the active sites of all Pd/Al_2O_3 catalysts are qualitatively similar and that TOF_{wet} is determined by the number of active sites. The higher activation energy under wet conditions compared to dry conditions (69–113 kJ mol^{-1})

also suggested that not only a C–H activation of CH_4, but also other steps were important for the CH_4 combustion in the presence of H_2O.[10] Furthermore, the effect of the partial pressure of each reaction gas on CH_4 combustion was examined (Figure S9), and the reaction orders with respect to CH_4 and O_2 were 0.55–1.1 and 0–0.2, respectively (Figures S10a and b). Therefore, it was suggested that the CH_4 combustion under wet conditions proceeds via the Mars-Van Krevelen mechanism, in which CH_4 is oxidized by the lattice oxygen of PdO.[29] In contrast, the reaction order with respect to H_2O ranged from −0.7 to −1.2 (Figure S10c), suggesting that at relatively low temperature (350 °C), the excess H_2O vapors inhibit the CH_4 combustion and the desorption of H_2O from the Pd catalyst may be the rate-limiting step of the reaction.[5,14,35]

2.7 In situ IR measurements

In situ infrared (IR) measurements were performed to observe adsorbed species on the surface of the Pd catalyst during CH_4 combustion. To eliminate the particle size effect, Pd/Al_2O_3 catalysts with the same Pd particle size were used. In the IR spectra of 7.3 nm $Pd/\theta\text{-}Al_2O_3$ exposed to an atmosphere of CH_4 combustion in the presence of H_2O, the band at around 3200–3800 cm^{-1} was attributed to the stretching vibration of OH/H_2O species adsorbed on the surface of the Pd catalyst (Figure 6b).[17,39–42] Particularly, the sharp IR bands at 3495 and 3549 cm^{-1} corresponded to the perturbed terminal OH group with hydrogen-interaction and triple bridge OH, respectively. In addition, a negative band was detected at 3770 cm^{-1}, which derived from the isolated OH group on the Al_2O_3 surface.[41,42] The vibration of the terminal OH group was suppressed due to the hydrogen-bond interaction between the hydrogen and the lone oxygen electron pairs of the adjacent OH/H_2O

species. The signal for gaseous H_2O was observed at 3500−3800 cm^{-1}.[13,17] However, the IR spectral shape of 7.3 nm Pd/θ-Al_2O_3 is clearly different from that of 9.3 nm Pd/α-Al_2O_3 (Figure 6c). Therefore, the H_2O in the gas phase is less contributed to the IR spectra than adsorbed OH/H_2O species on catalysts. Unfortunately, according to previous reports, the OH/H_2O species adsorbed on Al_2O_3 and PdO surfaces could not be distinguished.

After the injection of the reaction gas of CH_4 combustion, the IR bands derived from CO_2 that was generated by the CH_4 combustion could be detected at 2350 cm^{-1},[13,18,25] while the sharp IR bands together with some discrete peaks at 3015 cm^{-1} were attributed to gas CH_4.[13,18,25] Moreover, the band intensities of the OH/H_2O species adsorbed on the Pd catalyst gradually increased, while the band intensities of CO_2 gradually decreased over time. Based on Figure 7a, the IR intensity of OH/H_2O species on the Pd catalyst increased over time, whereas that of CO_2 was suppressed to half the initial intensity. Thus, the accumulation of OH/H_2O species on the Pd catalyst reduced the CH_4 combustion activity in the presence of H_2O. The time course obtained by the *in situ* IR measurements corresponded to the time course of the CH_4 conversion (Figure S5). Moreover, the IR spectrum of OH/H_2O species on 7.7 nm Pd/γ-Al_2O_3 (Figure 6a) was similar to that of the 7.3 nm Pd/θ-Al_2O_3 catalyst (Figure 6b). However, the IR band of CO_2 could not almost be detected due to the extremely low activity of the 7.7 nm Pd/γ-Al_2O_3 catalyst (TOF_{wet}: 0.005 s^{-1}). In addition, the 9.3 nm Pd/α-Al_2O_3 catalyst exhibited a broad IR band centered at 3400 cm^{-1} during CH_4 combustion (Figure 6c), while it reduced the CO_2 production with increasing the accumulation of OH/H_2O species on the catalyst

surface (Figure 7b). However, the deactivation percentage of 9.3 nm Pd/α-Al_2O_3 (ca. 35%) was lower than that of 7.3 nm Pd/θ-Al_2O_3 (ca. 60%). Further H_2O–D_2O exchange experiments during CH_4 combustion revealed that the OH/H_2O species reversibly adsorbed and desorbed on the Pd catalyst (Figure S11). In addition, the H_2O desorption–D_2O adsorption over 9.3 nm Pd/α-Al_2O_3 almost stopped after 2 min (Figure S11b), whereas that of Pd/θ-Al_2O_3 occurred for 5 min (Figure S11b). Consequently, the OH/H_2O species can adsorb and desorb more quickly on Pd/α-Al_2O_3 than on Pd/θ-Al_2O_3.

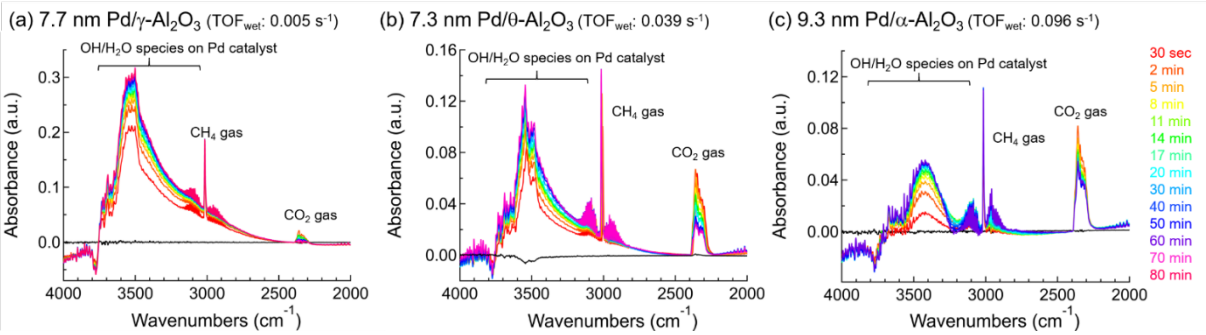

Figure 6. IR spectra of the (a) 7.7 nm Pd/γ-Al_2O_3, (b) 7.3 nm Pd/θ-Al_2O_3, and (c) 9.3 nm Pd/α-Al_2O_3 catalysts during CH_4 combustion under wet conditions (0.4% CH_4, 10% O_2, 3% H_2O, and Ar balance) at 350 °C.

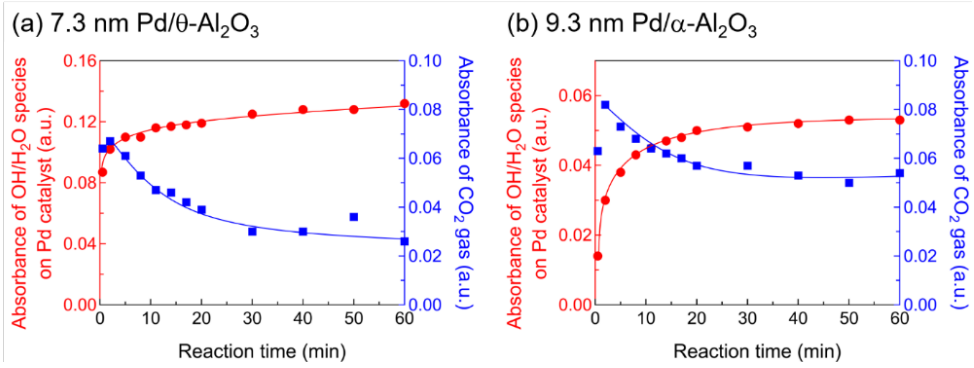

Figure 7. Change in the IR absorbance of OH/H_2O species on Pd catalysts and CO_2 gas over time.

2.8 H_2O-TPD of Al_2O_3 supports

The desorption of OH/H_2O species on the Al_2O_3 surface was measured by H_2O temperature-programmed desorption (H_2O-TPD). The desorption peaks of H_2O at around 150 °C were observed for all Al_2O_3 phases and shifted to higher temperatures in the order α-Al_2O_3 < θ-Al_2O_3 < γ-Al_2O_3. In addition, desorption peaks of H_2O were observed at >600 °C for γ-Al_2O_3 and θ-Al_2O_3. Although the assignment of the desorption peaks was difficult, the IR spectra of OH/H_2O adsorbed on θ-Al_2O_3 revealed that the desorption peaks of H_2O at around 150 and 600 °C (Figure 8) mainly derived from perturbed terminal OH groups with hydrogen-bond interactions (3491 cm^{-1}) and isolated triple bridge OH (3555 cm^{-1}), respectively (Figure S12). Figure S13 shows the IR spectra of the different Al_2O_3 phases in the OH/H_2O region after heat treatment at 500 °C under an inert gas. The IR bands observed for γ-Al_2O_3 and θ-Al_2O_3 at 3583 and 3675 cm^{-1} were attributed to the stretching vibration of the triple bridge and bridge OH group on the Al_2O_3.[41,42] The γ-Al_2O_3 and θ-Al_2O_3 surfaces with stable OH groups displayed stronger interactions with H_2O than with the α-Al_2O_3 surface. Furthermore, the amount of desorbed H_2O increased in the order α-Al_2O_3 < θ-Al_2O_3 < γ-Al_2O_3 (Table 1), and the findings for γ-Al_2O_3 complied with the results of a previous report.[13] From a thermodynamic point of view, the transition processes from oxide to hydroxide is $PdO + H_2O \rightleftarrows Pd(OH)_2$ with $\Delta G_{(623\ K)} = 60.6\ kJ/mol$, and $1/3\,Al_2O_3 + H_2O \rightleftarrows 2/3\,Al(OH)_3$ with $\Delta G_{(623\ K)} = 146.5\ kJ/mol$.[43] Moreover, the adsorption process of H_2O on the Al_2O_3 surface is $Al_2O_3 + H_2O \rightleftarrows H_2O@Al_2O_3$ with $\Delta G_{(623\ K)} = -\ 18\ kJ/mol$.[43] Thus, the OH/$H_2O$ species released from the Al_2O_3 surface can adsorb on the PdO surface or form inactive $Pd(OH)_2$ species.[12] While, the transformation of Al_2O_3 bulk to hydroxide was thermodynamically undesirable.

Consequently, the hydrophilic γ-Al_2O_3 or θ-Al_2O_3, which have a large amount of stable OH/H_2O species, can hinder the CH_4 combustion over PdO nanoparticles. Instead, the H_2O-poisoning on PdO nanoparticles is weak on the relatively hydrophobic α-Al_2O_3, where OH/H_2O species can easily desorb.

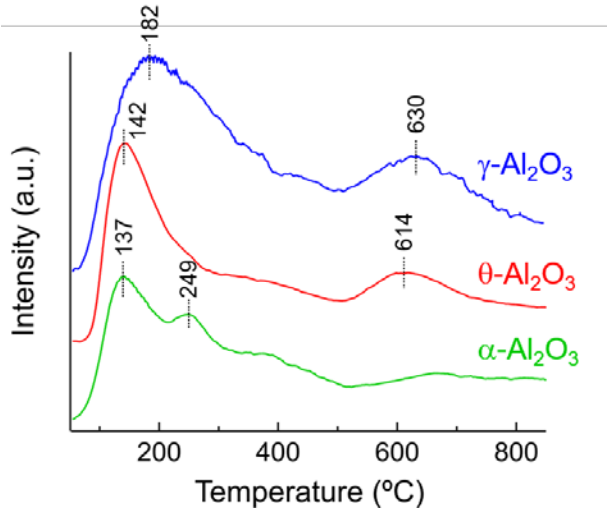

Figure 8. H_2O-TPD profiles of the Al_2O_3 supports. The sample amounts of γ-Al_2O_3, θ-Al_2O_3, and α-Al_2O_3 were 0.1, 1.0, and 4.0 g, respectively.

3. CONCLUSIONS

In this study, we investigated the effect of the Pd particle size and the Al_2O_3 crystalline phase on the CH_4 combustion in the presence of H_2O over Pd/Al_2O_3 catalysts. At Pd particle sizes lower than 7 nm, the activity increased monotonically with increasing Pd particle size, whereas above 7 nm the CH_4 combustion activity was almost constant. Amorphous-like PdO particles were mainly observed on Pd/Al_2O_3 with smaller Pd particle size. However, as the Pd particle size increased, highly crystalline PdO particles were formed on Al_2O_3, which were highly active species for CH_4 combustion in the presence of H_2O. In addition, the role of

the Al_2O_3 support on CH_4 combustion under wet conditions was elucidated by changing the Al_2O_3 crystalline phase. The CH_4 combustion activities of Pd/α-Al_2O_3 were higher than those of Pd/γ-Al_2O_3 and Pd/θ-Al_2O_3 irrespective of the Pd particle size. Moreover, comparison of the CH_4 combustion activities in the presence and absence of H_2O indicated that Pd/α-Al_2O_3 was clearly resistant to deactivation by H_2O, as the H_2O molecules adsorbed directly on the PdO surface and on the PdO particles via the Al_2O_3 surface. The adsorption/desorption of OH/H_2O species on the relatively hydrophobic α-Al_2O_3 phase was faster than that on γ-Al_2O_3 and γ-Al_2O_3, thus limiting the H_2O-poisoning on the active PdO species in the vicinity. Therefore, the CH_4 combustion activity of Pd/Al_2O_3 under wet conditions, which resembles the actual conditions in a catalytic converter, was significantly improved by using the hydrophobic α-Al_2O_3 support.

ASSOCIATED CONTENT

Supporting Information.

The following files are available free of charge.

Average Pd particle size of Pd/Al_2O_3 catalysts in the metallic state; the curve fitting results of Pd K-edge EXAFS spectra for the Pd/Al_2O_3 catalysts; comparison for methane conversion of Pd catalysts at 350 °C; dependence of the coordination number of Pd−Pd in PdO on the Pd particle size; the activity tests of CH_4 combustion over 2wt% Pd/Al_2O_3 catalysts under steady-state and temperature dependence of TOF_{wet} at 350 °C; plot of TOF_{wet} at 350 °C against the Δintensity of PdO derived from XRD pattern; plot of TOF_{wet} at 350

°C against the coordination number of Pd−Pd in PdO estimated by the curve fitting of Pd K-edge EXAFS spectra; plots of normalized TOF_{wet} of Pd/Al_2O_3 catalysts prepared via a colloidal method against reaction time; Pd K-edge XANES and FTs of EXAFS spectra for Pd/Al_2O_3 with different particle sizes; Arrhenius plots for CH_4 combustion under wet conditions over Pd/Al_2O_3 catalysts; plots of apparent activation energy for CH_4 combustion under wet conditions against Pd particle size; the dependence of TOF_{wet} on partial pressure of CH_4, O_2 and H_2O for CH_4 combustion under wet conditions over Pd/Al_2O_3 catalysts; plots of reaction order for CH_4 combustion under wet conditions against Pd particle size; IR spectra of Pd/Al_2O_3 catalyst during CH_4 combustion under wet conditions at 350 °C; IR spectra of OH/H_2O adsorbed on θ-Al_2O_3 pretreated under Ar at each temperature; and IR spectra of OH/H_2O adsorbed on Al_2O_3 pretreated under Ar at 500 °C (PDF)

AUTHOR INFORMATION

Corresponding Author

*E-mail: satsuma@chembio.nagoya-u.ac.jp.

Notes

Any additional relevant notes should be placed here.

ACKNOWLESGMENTS

This work was partly supported by the JSPS KAKENHI Grant-in-Aids for Scientific Research (B) (Grant Nos. 18H01787), Young Scientists (A) (Grant Nos. 16H06131), and JSPS Fellows (Grant Nos. 19J15440) from the Ministry of Education, Culture, Sports, Science and Technology (MEXT), Japan. A part of this work was managed by the Elements Strategy Initiative for Catalysts & Batteries (ESICB, JPMXP0112101003), which is also supported by MEXT. XAFS measurement was conducted at BL01B1 of SPring-8 (Approval No. 2017B0910). We thank Prof. Seiji Yamazoe for the XAFS measurement in the SPring-8. The authors would like to thank Enago (www.enago.jp) for the English language review.

ABBREVIATIONS

XAFS, X-ray absorption fine structure

XRD, X-ray diffraction

TPD, temperature-programmed desorption

IR, infrared

BET, Brunauer–Emmett–Teller

STEM, scanning transmission electron microscopy

XANES, X-ray absorption near edge structure

FTs, Fourier transforms

EXAFS, extended X-ray absorption structure

TOF_{wet}, turnover frequency of the catalysts under wet conditions

TOF_{dry}, turnover frequency of the catalysts under dry conditions

References

(1) Robert J. Farrauto. Low-Temperature Oxidation of Methane. *Science* **2012**, *337*, 659–660.

(2) Mahara, Y.; Tojo, T.; Murata, K.; Ohyama, J.; Satsuma, A. Methane Combustion over $Pd/CoAl_2O_4/Al_2O_3$ Catalysts Prepared by Galvanic Deposition. *RSC Adv.* **2017**, *7*, 34530–34537.

(3) Chin, Y. H. C.; García-Diéguez, M.; Iglesia, E. Dynamics and Thermodynamics of Pd-PdO Phase Transitions: Effects of Pd Cluster Size and Kinetic Implications for Catalytic Methane Combustion. *J. Phys. Chem. C* **2016**, *120*, 1446–1460.

(4) Matam, S. K.; Aguirre, M. H.; Weidenkaff, A.; Ferri, D. Revisiting the Problem of Active Sites for Methane Combustion on Pd/Al_2O_3 by Operando XANES in a Lab-Scale Fixed-Bed Reactor. *J. Phys. Chem. C* **2010**, *114*, 9439–9443.

(5) Willis, J. J.; Gallo, A.; Sokaras, D.; Aljama, H.; Nowak, S. H.; Goodman, E. D.; Wu, L.; Tassone, C. J.; Jaramillo, T. F.; Abild-pedersen, F.; Cargnello, M. Systematic Structure−Property Relationship Studies in

Palladium-Catalyzed Methane Complete Combustion. *ACS Catal.* **2017**, *7*, 7810–7821.

(6) Duan, H.; You, R.; Xu, S.; Li, Z.; Qian, K.; Cao, T.; Huang, W.; Bao, X. Penta-Coordinated Al^{3+} Stabilized Active Pd Structures on Al_2O_3 Coated Palladium Catalysts for Methane Combustion. *Angew. Chemie Int. Ed.* **2019**, *58*, 12043–12048.

(7) Yang, X.; Li, Q.; Lu, E.; Wang, Z.; Gong, X.; Yu, Z.; Guo, Y.; Wang, L.; Guo, Y.; Zhan, W.; Zhang, J.; Dai, S. Taming the Stability of Pd Active Phases through a Compartmentalizing Strategy toward Nanostructured Catalyst Supports. *Nat. Commun.* **2019**, *10*, 1611.

(8) Yoshida, H.; Nakajima, T.; Yazawa, Y.; Hattori, T. Support Effect on Methane Combustion over Palladium Catalysts. *Appl. Catal. B Environ.* **2007**, *71*, 70–79.

(9) Murata, K.; Kosuge, D.; Ohyama, J.; Mahara, Y.; Yamamoto, Y.; Arai, S.; Satsuma, A. Exploiting Metal−Support Interactions to Tune the Redox Properties of Supported Pd Catalysts for Methane Combustion. *ACS Catal.* **2020**, *10*, 1381–1387.

(10) Murata, K.; Mahara, Y.; Ohyama, J.; Yamamoto, Y.; Arai, S.; Satsuma, A. The Metal-Support Interaction Concerning the Particle Size Effect of Pd/Al_2O_3 on Methane Combustion. *Angew. Chemie Int. Ed.* **2017**, *56*, 15993–15997.

(11) Gholami, R.; Alyani, M.; Smith, K. Deactivation of Pd Catalysts by Water during Low Temperature Methane Oxidation Relevant to Natural Gas Vehicle Converters. *Catalysts* **2015**, *5*, 561–594.

(12) Barrett, W.; Shen, J.; Hu, Y.; Hayes, R. E.; Scott, R. W. J.; Semagina, N. Understanding the Role of SnO_2

Support in Water-tolerant Methane Combustion: In Situ Observation of $Pd(OH)_2$ and Comparison with Pd/Al_2O_3. *ChemCatChem* **2019**, *11*, 1–10.

(13) Losch, P.; Huang, W.; Vozniuk, O.; Goodman, E. D.; Schmidt, W.; Cargnello, M. Modular Pd/Zeolite Composites Demonstrating the Key Role of Support Hydrophobic/Hydrophilic Character in Methane Catalytic Combustion. *ACS Catal.* **2019**, 4742–4753.

(14) Ciuparu, D.; Pfefferle, L. Support and Water Effects on Palladium Based Methane Combustion Catalysts. *Appl. Catal. A Gen.* **2001**, *209*, 415–428.

(15) Li, X.; Wang, X.; Roy, K.; Bokhoven, J. A. Van; Artiglia, L. Role of Water on the Structure of Palladium for Complete Oxidation of Methane. *ACS Catal.* **2020**, *10*, 5783–5792.

(16) Coney, C.; Stere, C. E.; Millington, P.; Raj, A.; Wilkinson, S.; Caracotsios, M.; McCullough, G.; Hardacre, C.; Morgan, K.; Thompsett, D.; goguet, alexandre. Spatially-Resolved Investigation of the Water Inhibition of Methane Oxidation over Palladium. *Catal. Sci. Technol.* **2020**.

(17) Schwartz, W. R.; Ciuparu, D.; Pfefferle, L. D. Combustion of Methane over Palladium-Based Catalysts: Catalytic Deactivation and Role of the Support. *J. Phys. Chem. C* **2012**, *116*, 8587–8593.

(18) Schwartz, W. R.; Pfefferle, L. D. Combustion of Methane over Palladium-Based Catalysts: Support Interactions. *J. Phys. Chem. C* **2012**, *116*, 8571–8578.

(19) Ciuparu, D.; Bozon-Verduraz, F.; Pfefferle, L. Oxygen Exchange between Palladium and Oxide Supports in Combustion Catalysts. *J. Phys. Chem. B* **2002**, *106*, 3434–3442.

(20) Alyani, M.; Smith, K. J. Kinetic Analysis of the Inhibition of CH_4 Oxidation by H_2O on PdO/Al_2O_3 and $CeO_2/PdO/Al_2O_3$ Catalysts. *Ind. Eng. Chem. Res.* **2016**, *55*, 8309–8318.

(21) Petrov, A. W.; Ferri, D.; Krumeich, F.; Nachtegaal, M.; Van Bokhoven, J. A.; Kröcher, O. Stable Complete Methane Oxidation over Palladium Based Zeolite Catalysts. *Nat. Commun.* **2018**, *9*, 2545.

(22) Petrov, A. W.; Ferri, D.; Tarik, M.; Kröcher, O.; van Bokhoven, J. A. Deactivation Aspects of Methane Oxidation Catalysts Based on Palladium and ZSM-5. *Top. Catal.* **2017**, *60*, 123–130.

(23) Chen, C.; Yeh, Y.; Cargnello, M.; Murray, C. B.; Fornasiero, P.; Gorte, R. J. Methane Oxidation on $Pd@ZrO_2/Si–Al_2O_3$ Is Enhanced by Surface Reduction of ZrO_2. *ACS Catal.* **2014**, *4*, 3902–3909.

(24) Park, J. H.; Cho, J. H.; Kim, Y. J.; Kim, E. S.; Han, H. S.; Shin, C. H. Hydrothermal Stability of Pd/ZrO_2 Catalysts for High Temperature Methane Combustion. *Appl. Catal. B Environ.* **2014**, *160–161*, 135–143.

(25) Dai, Q.; Zhu, Q.; Lou, Y.; Wang, X. Role of BrØnsted Acid Site during Catalytic Combustion of Methane over PdO/ZSM-5: Dominant or Negligible? *J. Catal.* **2018**, *357*, 29–40.

(26) Kikuchi, R.; Maeda, S.; Sasaki, K.; Wennerström, S.; Eguchi, K. Low-Temperature Methane Oxidation over Oxide-Supported Pd Catalysts: Inhibitory Effect of Water Vapor. *Appl. Catal. A Gen.* **2002**, *232*, 23–28.

(27) Wischert, R.; Copéret, C.; Delbecq, F.; Sautet, P. Optimal Water Coverage on Alumina: A Key to Generate Lewis Acid-Base Pairs That Are Reactive towards the C-H Bond Activation of Methane. *Angew. Chem. Int. Ed.* **2011**, *50*, 3202–3205.

(28) Busca, G. The Surface of Transitional Aluminas: A Critical Review. *Catal. Today* **2014**, *226*, 2–13.

(29) Chin, Y.-H. C.; Buda, C.; Neurock, M.; Iglesia, E. Consequences of Metal-Oxide Interconversion for C-H Bond Activation during CH_4 Reactions on Pd Catalysts. *J. Am. Chem. Soc.* **2013**, *135*, 15425–15442.

(30) Zhang, F.; Hakanoglu, C.; Hinojosa, J. A.; Weaver, J. F. Inhibition of Methane Adsorption on PdO(101) by Water and Molecular Oxygen. *Surf. Sci.* **2013**, *617*, 249–255.

(31) Mahara, Y.; Murata, K.; Ueda, K.; Ohyama, J.; Kato, K.; Satsuma, A. Time Resolved in Situ DXAFS Revealing Highly Active Species of PdO Nanoparticle Catalyst for CH_4 Oxidation. *ChemCatChem* **2018**, *10*, 3384–3387.

(32) Murata, K.; Eleen Eleeda; Ohyama, J.; Yamamoto, Y.; Arai, S.; Satsuma, A. Identification of Active Sites in CO Oxidation over a Pd/Al_2O_3 Catalyst. *Phys. Chem. Chem. Phys.* **2019**, *21*, 18128–18137.

(33) Goodman, E. D.; Dai, S.; Yang, A.-C.; Wrasman, C. J.; Gallo, A.; Bare, S. R.; Hoffman, A. S.; Jaramillo, T. F.; Graham, G. W.; Pan, X.; Cargnello, M. Uniform Pt/Pd Bimetallic Nanocrystals Demonstrate Platinum Effect on Palladium Methane Combustion Activity and Stability. *ACS Catal.* **2017**, 4372–4380.

(34) Nassiri, H.; Lee, K. E.; Hu, Y.; Hayes, R. E.; Scott, R. W. J.; Semagina, N. Water Shifts PdO-Catalyzed Lean Methane Combustion to Pt-Catalyzed Rich Combustion in Pd–Pt Catalysts: In Situ X-Ray Absorption Spectroscopy. *J. Catal.* **2017**, *352*, 649–656.

(35) Bossche, M. Van den; Grönbeck, H. Methane Oxidation over PdO(101) Revealed by First-Principles Kinetic Modeling. *J. Am. Chem. Soc.* **2015**, *137*, 12035–12044.

(36) Keating, J.; Sankar, G.; Hyde, T. I.; Kohara, S.; Ohara, K. Elucidation of Structure and Nature of the

PdO-Pd Transformation Using in Situ PDF and XAS Techniques. *Phys. Chem. Chem. Phys.* **2013**, *15*, 8555–8565.

(37) Price, R.; Eralp-Erden, T.; Crumlin, E.; Rani, S.; Garcia, S.; Smith, R.; Deacon, L.; Euaruksakul, C.; Held, G. The Partial Oxidation of Methane over Pd/Al2O3 Catalyst Nanoparticles Studied In-Situ by Near Ambient-Pressure X-Ray Photoelectron Spectroscopy. *Top. Catal.* **2016**, *59*, 516–525.

(38) Gabasch, H.; Hayek, K.; Klötzer, B.; Unterberger, W.; Kleimenov, E.; Teschner, D.; Zafeiratos, S.; Hävecker, M.; Knop-Gericke, A.; Schlögl, R.; Aszalos-Kiss, B.; Zemlyanov, D. Methane Oxidation on Pd(111): In Situ XPS Identification of Active Phase. *J. Phys. Chem. C* **2007**, *111*, 7957–7962.

(39) Ciuparu, D.; Perkins, E.; Pfefferle, L. In Situ DR-FTIR Investigation of Surface Hydroxyls on γ-Al_2O_3 Supported PdO Catalysts during Methane Combustion. *Appl. Catal. A Gen.* **2004**, *263*, 145–153.

(40) Persson, K.; Pfefferle, L. D.; Schwartz, W.; Ersson, A.; Järås, S. G. Stability of Palladium-Based Catalysts during Catalytic Combustion of Methane: The Influence of Water. *Appl. Catal. B Environ.* **2007**, *74*, 242–250.

(41) Velin, P.; Ek, M.; Skoglundh, M.; Schaefer, A.; Raj, A.; Thompsett, D.; Smedler, G.; Carlsson, P. A. Water Inhibition in Methane Oxidation over Alumina Supported Palladium Catalysts. *J. Phys. Chem. C* **2019**, *123*, 25724–25737.

(42) Digne, M.; Sautet, P.; Raybaud, P.; Euzen, P.; Toulhoat, H. Use of DFT to Achieve a Rational Understanding of Acid-Basic Properties of γ-Alumina Surfaces. *J. Catal.* **2004**, *226*, 54–68.

(43) Huang, W.; Goodman, E. D.; Losch, P.; Cargnello, M. Deconvoluting Transient Water Effects on the Activity of Pd Methane Combustion Catalysts. *Ind. Eng. Chem. Res.* **2018**, *57*, 10261–10268.